

WEAKNESS OF THE AIR-SEA THERMAL COUPLING DURING INDIAN OCEAN DIPOLE MODE IN THE 1990S

Masanori Konda^{1*}, Hiroyuki Kobayashi¹, Takashi Mochizuki², and Motoki Nagura³

1: Department of Geophysics, Graduate School of Geophysics, Kyoto University, Kyoto, Japan

2: JAMSTEC/ Frontier Research Center for Global Change, Yokohama, Kanagawa, Japan

3: NOAA/ Pacific Marine Environmental Laboratory, Seattle, WA, USA

1. INTRODUCTION

It is known that the Indian Ocean sea surface temperature (SST) anomaly shows the zonal dipole pattern in fall (Hastenrath et al. 1993; Harrison and Larkin 1998; Saji et al. 1999; Webster et al. 1999). The development of this phenomenon, which is called Indian Ocean Dipole mode (IOD), has the deeply fixed on the calendar month; i.e., the SST anomaly in the equatorial eastern Indian Ocean (EEIO) in May is enlarged both in magnitude and space until September. (Saji et al. 1999; Annamalai et al. 2003; Kajikawa et al. 2003) It tends to disappear by the reversal of the SST anomaly in the east by the end of the year. Saji et al. (1999) defined the Dipole Mode Index (DMI) as the difference between the SST anomalies in the east and the west portion of the equatorial Indian Ocean for the proxy of IOD.

It has been considered that the seasonal development of IOD is strongly influenced by the change of the atmospheric circulation (Li et al. 2002; Hendon 2003; Shinoda et al. 2004; Lau and Nath 2004, Nagura and Konda 2007). The correlation between the change of the SST anomaly in the EEIO and the wind anomaly shows the good correspondence suggesting the strong air-sea coupling processes. On the other hand, some studies suggest the important role of oceanic processes such as the wave propagation or the

coastal upwelling (Vinayachandran et al. 2002; McClean et al. 2005; Sakova et al. 2006). These studies seem to indicate the sea surface and the oceanic process work on the generation of IOD through the anomalous wind speed in the EEIO in May.

However, the relative importance of individual processes is not evaluated well. Previous studies tends to compare the physical parameters with the DMI by the spatial averaging in the eastern or the western pole region defined by Saji et al.(1999). They assume that the physical process causes the change of the SST anomaly dominates everywhere in the each pole. It is needed to evaluate temporal and spatial changes of the SST anomalies in the DMI region in detail in order to know which physical process dominates the ocean temperature anomaly in each pole.

For this analysis, the difficulty lies on the lack of oceanic information such as the mixed layer depth. The temperature profile in the EEIO in the air-sea coupled model might give us the information about the oceanic temperature profile affected by the strong air-sea interaction. Shinoda et al. (2004) analyzed an air-sea coupled model forced by the El Niño SST anomaly in the tropical Pacific. However, the amplitude of the SST anomaly is much smaller than the observation. It might be because of the limitation of the one dimensional ocean model as it can not reproduce the effect of the oceanic wave nor the coastal upwelling at al.

Recently, a coupled data assimilation technique is developed by Japan Agency for Marine-Earth Science and Technology (JAMSTEC) K7 project (Sugiura et al. 2008; Mochizuki et al. 2009). It is a

Corresponding author address: Masanori Konda, Dept. of Geophysics, Grad. Sch. of Science, Kyoto University, Kitashirakawa-Oiwake, Sakyo, Kyoto-city, Kyoto 606-8502, Japan; e-mail: konda@kugi.kyoto-u.ac.jp

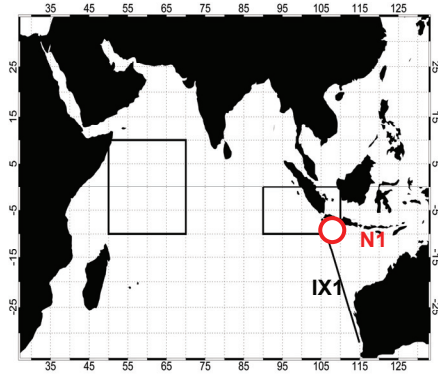


Figure 1: The east and the west poles for the DMI in the equatorial Indian Ocean (squares). The IX1 repeat XBT section is indicated by the solid line between Java island and the southwest coast of Australia. The northernmost point of the IX1 (106E, 8S) used for the point analysis is also shown by the red circle (N1).

kind of comprehensive data set, which can reproduce the physically consistent oceanic and atmospheric data set, reflecting the coupling process. In addition, the observation can give us a truth data even if it does not sufficient in time and space. A ten years expendable bathythermograph (XBT) observation during 1990s contains two typical IOD events and can provide us the information of the oceanic temperature profile almost every month (Meyers 1996; Feng and Meyers 2001; Sakova et al. 2006).

In this paper, we will evaluate the relative importance of the processes concerning the generation and the development of IOD, by considering results of observational and assimilated data sets together. We will suggest that the coastal upwelling mainly controls the occurrence of IOD and that the contribution of the air-sea coupling process is much weaker than we believed.

2. DATA

We use the observation of the ocean temperature of 10 years (1990-1999) of the World Ocean Circulation Experiment (WOCE) repeat IX1 (XBT) section between Java and Western Australia (Fig. 1). The cruises of the section are almost one or two times a month. As the frequency and the spatial gap of every XBT deployments of the individual cruise is irregular,

we make the monthly data with 1 degree resolution by the simple boxcar average. The sampling frequency of the XBT data is tabulated in Table 1. In addition, we will use the monthly surface heat flux data of the NCEP-NCAR reanalysis data set (Kalnay et al. 1996) for the one dimensional heat budget analysis using the XBT profile.

We define the temporal anomaly of the physical parameters as the deviation from the mean annual cycle from 1990 to 1999. The eastern and the western pole region to compute the DMI is defined as boxes in the EEIO (90°E - 110°E, 0° - 10°S) and the equatorial western Indian Ocean (50°E - 70°E, 10°N - 10°S) according to Saji et al.(1999) (Fig. 1). The DMI is defined as the difference between the SST anomalies averaged in the eastern pole and the western pole. IOD is considered to occur when the DMI from September to November exceeds the standard deviation of the mean annual cycle (0.39°C in this study). The positive IOD occurs in 1991, 1994 and 1997, whereas the negative IOD does in 1992, 1996 and 1998 according to the definition. We compute the composites of the positive and the negative IODs for the simplicity.

The oceanic and atmospheric data are obtained by Coupled Four-Dimensional Variational analysis system (Coupled 4D-VAR) developed by JAMSTEC K7 project (Sugiura et al. 2008; Mochizuki et al. 2009). The data exists from January in 1990 to December 1999. The monthly average ocean temperature and the other oceanic and meteorological parameters such as the wind and the surface heat flux with one degree resolution are used

Table 1: IX1 line sampling frequency from 1990 to 1999.

year	90	91	92	93	94	95	96	97	98	99	total
jan	2	2	3	2	2	2	2	2	1	2	20
feb	2	2	2	2	4	2	2	2	1	3	22
mar	2	4	1	3	3	2	1	3	0	3	22
apr	2	3	2	2	2	4	2	2	2	3	24
may	3	2	2	3	3	3	2	1	2	2	23
jun	2	2	3	2	1	2	4	2	3	2	23
jul	3	2	2	2	3	2	2	3	0	1	20
aug	2	2	2	2	1	2	0	2	0	1	14
sep	2	3	2	2	1	2	1	2	2	2	19
oct	2	2	2	2	2	2	2	2	1	1	18
nov	2	2	2	2	2	3	2	2	2	2	21
dec	2	2	2	2	2	2	2	3	2	2	21
total	26	28	25	26	26	28	22	26	16	24	247

for the analysis. The vertical resolution of the ocean temperature near the sea surface is almost 10m.

Figure 3 shows composites of the temperature anomaly cross section of the 4D-VAR system. It is found that the temperature anomaly is well reproduced in the Coupled 4D-VAR system. For example, the temperature anomaly maximum below the sea surface in July and November is quite similar, although the amplitude is slightly weak possibly because of the large diffusivity in the system. We consider that the temperature data of the Coupled 4D-VAR system can be used for the analysis of the IOD development, judging from the agreement of the temperature profile of the Coupled 4D-VAR system with the XBT observation.

We will use the satellite-based SST data (Reynolds et al. 2007) for an independent analysis of the change of the SST anomaly in the EEIO.

3. HEAT BUDGET ANALYSIS BASED ON THE XBT OBSERVATION

We will investigate the one dimensional heat budget in the eastern pole of IOD as the early stage of the development of IOD almost depends on the SST anomaly in the eastern pole (Nagura and Konda 2007). The relationship between the ocean temperature profile and the surface heat flux at the

northernmost point of the IX1 (106°E, 8°S) near the south coast of Java (N1) is analyzed using the XBT data and the NCEP-NCAR reanalysis data set. This point is selected because the composite of the temperature cross section along IX1 shows that the temperature anomaly is the maximum in the south coast of Java (Fig. 2). Fig.2 also shows that the temperature anomaly in the positive and the negative IOD years is the largest in the thermocline depth of about 100m below the sea surface.

One dimensional heat budget at N1 is diagnosed using the XBT temperature profile and the surface heat flux of the NCAR reanalysis data. The change of the heat storage in the mixed layer is computed by eq.(1),

$$\begin{aligned} \frac{1}{\rho C_p} (Q_{flux} + Q_{ent} + Q_{adv}) \\ = \frac{\partial}{\partial t} (T_{mld} H) \\ = \frac{\partial T_{mld}}{\partial t} H + T_{mld} \frac{\partial H}{\partial t} \end{aligned} \quad (1)$$

,where

$$\frac{\partial T_{mld}}{\partial t} = \frac{1}{\rho CH} (Q_{flux} + Q_{ent} + Q_{adv}) - \frac{T_{mld}}{H} \frac{\partial H}{\partial t} \quad (2).$$

The heat flux at the sea surface and the bottom of

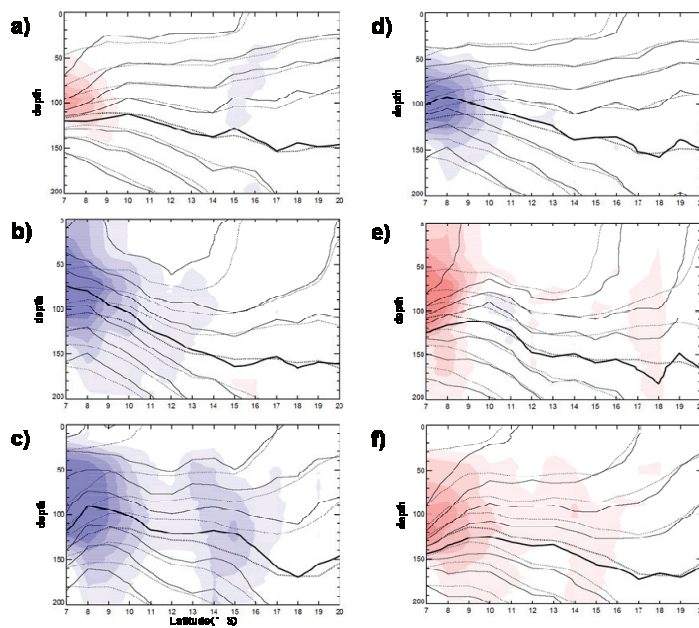


Figure 2: The composites of the temperature anomaly cross section (color) along the IX1 in a) January-February, b) July-August and c) November-December in the positive dipole years. The vertical axis shows the depth from the sea surface to 200m. The horizontal axis shows the latitude from 7°S to 20°S from the left to the right. The blue (red) color indicates the negative (positive) value with every 0.5°C intervals. The climatological mean temperature is superimposed by the contour. The interval of the climatological temperature is 2 °C with the thick line at 20 °C isotherm. The composites in the negative IOD years are shown in panels d), e) and f).

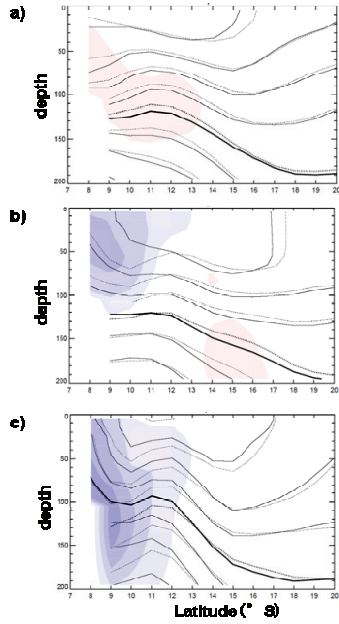


Figure 3: Same as Figure 2 a to c except for the temperature data derived from the 4D-VAR system instead of the observation.

the mixed layer is indicated by Q_{flux} and Q_{ent} respectively.

The horizontal heat flux caused by the advection is shown by Q_{adv} . T_{mld} shows the temperature averaged in the mixed layer, and H the mixed layer depth. The density of the sea water (ρ) is assumed to be $1.0 \times 10^3 \text{ kgm}^{-3}$, and the specific heat C_p to be $4.2 \times 10^3 \text{ JKkg}^{-1}$. Dividing the first term in eq.(2) into the mean annual cycle and the anomaly becomes

$$\begin{aligned} & \frac{1}{\rho C_p} (\overline{Q_{flux}} + \overline{Q_{flux}'} + \overline{Q_{ent}} + \overline{Q_{ent}'} + \overline{Q_{adv}} + \overline{Q_{adv}'}) \\ &= \frac{\alpha (\overline{T_{mld}} + \overline{T_{mld}'}) (\overline{H} + \overline{H}') + (\overline{T_{mld}} + \overline{T_{mld}'}) \frac{\alpha (\overline{H} + \overline{H}')}{\alpha}}{\alpha} \\ &\approx \frac{\partial \overline{T_{mld}}}{\partial \alpha} \overline{H} + \frac{\partial \overline{T_{mld}}}{\partial \alpha} \overline{H}' + \frac{\partial \overline{T_{mld}}}{\partial \alpha} \overline{H} \\ &\quad + \overline{T_{mld}} \frac{\partial \overline{H}}{\alpha} + \overline{T_{mld}} \frac{\partial \overline{H}'}{\alpha} + \overline{T_{mld}'} \frac{\partial \overline{H}}{\alpha} \end{aligned}$$

(3),

where

$$\frac{\partial \overline{T_{mld}}}{\partial t} = \frac{1}{\rho C_p H} (\overline{Q_{flux}} + \overline{Q_{ent}} + \overline{Q_{adv}}) - \underbrace{\frac{\overline{T_{mld}}}{H} \frac{\partial \overline{H}}{\partial t}}_{D4}$$

(4),

and

$$\begin{aligned} \frac{\partial T_{mld}'}{\partial t} &\approx \frac{1}{\rho C_p H} (\overline{Q_{flux}'} + \overline{Q_{ent}'} + \overline{Q_{adv}'}) \\ &\quad - \underbrace{\frac{H'}{H} \frac{\partial \overline{T_{mld}}}{\partial t}}_{D5} - \underbrace{\frac{\overline{T_{mld}}}{H} \frac{\partial H'}{\partial t}}_{E5} - \underbrace{\frac{\overline{T_{mld}}}{H} \frac{\partial \overline{H}}{\partial t}}_{F5} \end{aligned}$$

(5).

The mean annual cycle is shown by the line over the variables and the anomaly is by dashes. The sum of terms A4(5), B4(5) and C4(5) in eq.4(5) indicates the anomalous net heat transfer into the ocean mixed layer. D4 indicates the contribution of the seasonal change of the mixed layer depth to the annual change of the mixed layer temperature. D5 indicates the anomalous change of the heat storage due to the anomaly of the mixed layer depth. The sum of E5 and F5 shows the contribution of the change rate of the mixed layer depth.

Figure 4 shows contributions of the individual terms in eq.(4) to the climatologically annual cycle of the mixed layer temperature. The sum of B4 and C4, the contribution of the entrainment and the advection, is obtained as the residual of the other terms in eq.(4). Fig. 4 clearly shows the climatology of the time change of the mixed layer temperature is almost attributable to the heat input at the sea surface. On

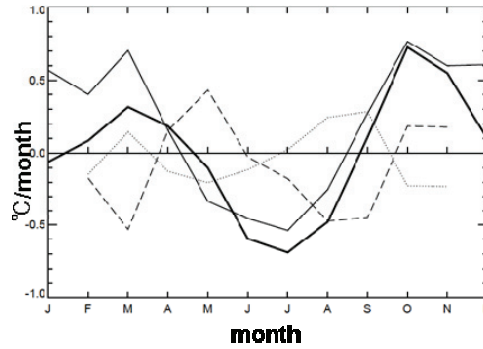


Figure 4: The term balance of eq.(4) explaining the climatology of the change of the mixed layer temperature anomaly at N1 (thick solid line). The terms A4 (solid line), D4 (gray line), and the sum of B4 and C4 (broken line) in eq.(4) are also shown. The time change is computed from the central differences between three consecutive values.

the other hand, the effect of the change of the mixed layer depth, and therefore the heat content (D4) and the sum of the advection and the entrainment (B4+C4) are in balance after June. Before May, the contribution of the entrainment and the advection has an effect to weaken the thermal forcing at the sea surface.

In contrast, the time change of the mixed layer temperature anomaly in IOD years is mainly dominated by the oceanic process while IOD is developing. Figure 5 shows the composite of the anomalous heat budget at the N1 according to eq.(5). The solid line and the broken line are almost balanced from May to July in the positive IOD year, indicating the ocean mixed layer is anomalously cooled by the oceanic processes such as the advection, and the entrainment caused by the seasonal and the anomalous changes of the mixed layer depth. Surprisingly, the contribution of the

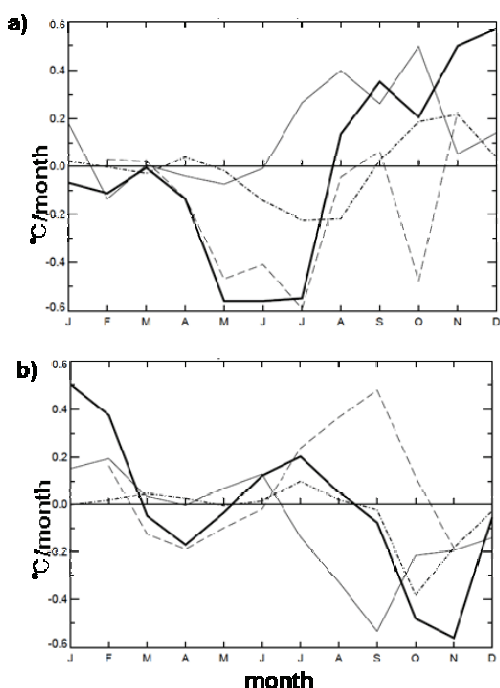


Figure 5: The term balance of eq.(5) explaining the time change of the mixed layer temperature anomaly (thick solid line) in a) the positive and b) the negative IOD years. The terms A5 (solid line), D5 (dotted line), and the the sum of B5, C5, E5 and F5 (broken line) in eq.(5) are also shown. The time change is computed from the central differences between three consecutive values.

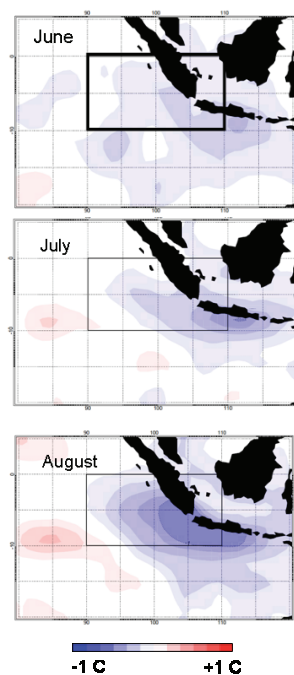


Figure 6: The SST anomaly composite in (up) June, (middle) July and (bottom) August in the positive IOD years derived from the Reynolds SST. The blue (red) color shows the negative (positive) anomaly.

surface heat input is not only small but also in opposite sign in June and July. After August, the disappearance of the positive IOD might be significantly affected by the surface warming.

The heat budget analysis at N1 (the south coast of Java) shows that the surface heat flux has the negative effect on the development of the IOD pattern during spring and summer. Considering that the maximum temperature anomaly is seen at the depth of the thermocline (Fig. 2), the heat budget analysis strongly suggests the dominant effect of the coastal upwelling in the early stage of the development of IOD in the coastal portion in the eastern pole region.

Whether the SST anomaly at N1 can be a representative of the eastern part of the DMI is investigated by the relationship between the SST anomaly at N1 and those in the other portions in the eastern pole. Figure 6 shows the satellite-based SST anomaly in the EEIO in the positive dipole years. The evolution of the spatial distribution of the SST anomaly shows that the SST anomaly at first

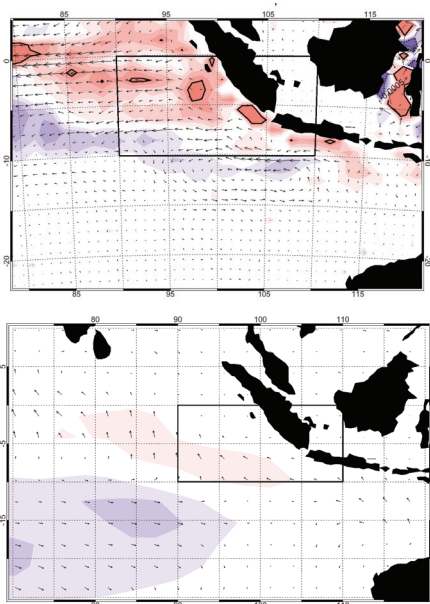


Figure 7: (a) The vertical velocity anomaly (color) and the horizontal velocity field (arrows) in May in the IOD years. The difference between the positive and the negative dipole years is drawn. (b) The wind speed anomaly (color) and the wind vector (arrows) in May. Red (blue) color indicates the positive (negative) anomaly.

appears along the coast of Java and expands to the offshore region. The maximum value is found along the coast of Java. The spatial pattern indicates that the SST anomaly caused by the coastal upwelling is transferred to the offshore region. Possibly, the SST anomaly along the south coast of Java dominates that in the whole region of the eastern pole.

4. ANALYSIS USING COUPLED 4D-VAR DATA

As we showed that the SST anomaly in the eastern pole region during the development of IOD has the quite close relationship not with the surface heat flux but with the coastal upwelling, we analyze the oceanic temperature data obtained by the Coupled 4D-VAR system. Figure 7 (a) shows the upward velocity anomaly in May averaged in the upper 50m in the EEIO. The difference between the positive and the negative IOD is displayed for the purpose of the exaggeration of the spatial pattern. We can see the strong upwelling along the coast of Java. It is found that the upwelling is associated with the alongshore

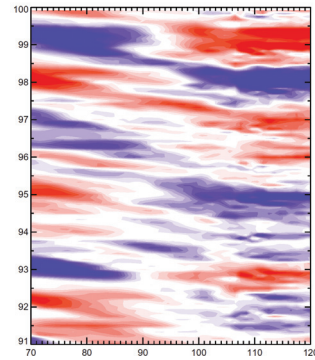


Figure 8: A Hovmöller diagram of the temperature anomaly averaged in the upper 100m along 8°S from 1991 to 1999.

wind anomaly as shown in Fig.7 (b). A Hovmöller analysis of the temperature anomaly shows the westward propagation of the temperature anomaly along the coast of Java is seen in both the SST and the upper 100m temperature average in the phase speed corresponding to the typical first baroclinic Rossby wave (Fig. 8).

5. DISCUSSION

Results in preceding sections should indicate the SST anomaly in the eastern pole region for the DMI is attributable to the coastal upwelling and its westward propagation due to the planetary wave. The difference between the result in this study and those in the previous studies should be discussed here. The previous studies, which mentioned the importance of the air-sea thermal coupling, are based on the correlation analysis between the spatial average of the DMI, the SST or the wind in the DMI areas regardless of the variability in the east pole area.

However, as we mentioned previously, there is a difference of the dominant process to change the SST anomaly between the coastal and offshore regions. In the same way, there is a possibility that strength of the air-sea coupling can change according to the relationship between the SST and the surface heat flux in the coastal and offshore regions.

Panels (a) and (b) in Fig. 9 respectively show the positive dipole composite of the net surface heat flux

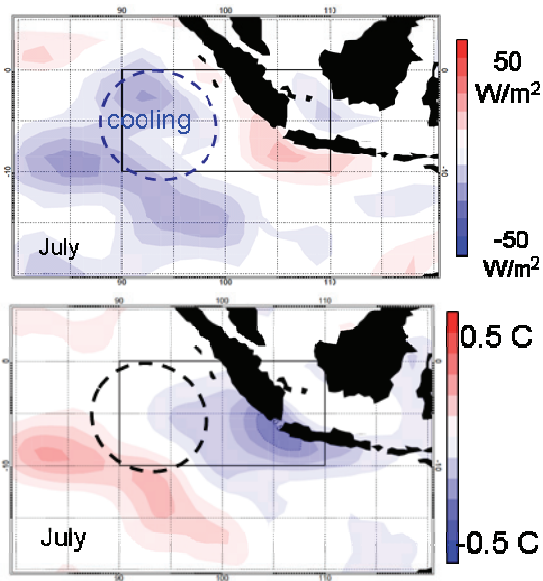


Figure 9: (top) Positive dipole composite of the net surface heat flux and (bottom) the time change of the SST anomaly in May. The dashed circle indicates the region, where the surface is cooled but the SST does not change significantly.

derived by NCEP-NCAR reanalysis and the time change of the SST in July. It is evident that the surface heat flux anomaly is warming the sea surface, while the SST is cooled along the coast of Java. In contrast, the surface heat flux cools the sea surface, while the SST is not changing in the month. Taking into account of the southeasterly anomaly in spring in the positive IOD years, the evaporative cooling is enhanced in the offshore region because

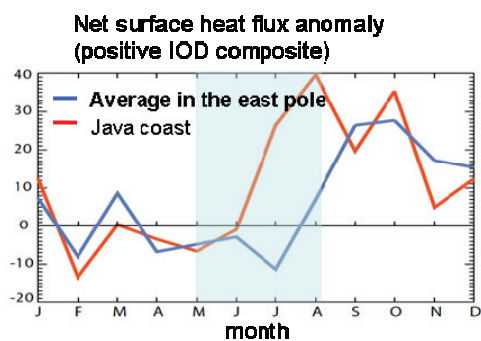


Figure 10: A Hovmöller diagram of the temperature anomaly averaged in the upper 100m along 8°S from 1991 to 1999.

of the increase of the wind speed without the small SST anomaly, while it is depressed because of the negative SST anomaly making the air-sea temperature difference small in the south Java coast. There is a reversal of the air-sea interaction between the coastal and the offshore regions.

Figure 10 shows the composite of the net surface heat flux at the N1 and that averaged in the whole eastern pole region. The variation of the surface flux is almost attributable to that of the latent heat flux in Fig. 10. Although the surface heat flux is positive while the SST anomaly along the south coast of Java is decreasing, the spatial average in the eastern pole region virtually generate the negative heat flux at the sea surface because of the negative heat flux in the offshore region (Fig. 9). As a consequent, there is no place where the sea and the atmosphere are thermally coupled, in the DMI east pole region. Averaging the physical parameters in the DMI regions might be misleading in this case.

6. SUMMARY

We analyzed the temporal and spatial variation of the thermal structure of the EEIO associated with IOD, mainly using the water temperature of 10 years (1990-1999) of the WOCE repeat IX1 XBT section between Java and Western Australia together with the product of the air-sea coupled 4D-VAR system. The temperature anomaly of the XBT section reveals that the change in the subsurface ocean temperature occurs earlier than that at the surface associated with IOD. From May to August, a marked subsurface temperature anomaly is also found as well as the SST associated with the wind anomaly along the Java coast. Heat budget analysis along IX1 shows that the surface heat flux does not dominate the mixed layer temperature anomaly near the south Java coast, but the change of the coastal upwelling mainly controls it.

Coupled 4D-VAR reproduces the anomalous upwelling velocity and the upward shift of the thermocline depth, associated with the southeasterly wind anomaly. Both surface and subsurface temperature anomalies in the eastern pole region seem to be transferred from the south Java coast

nearly at the speed of the first baroclinic Rossby wave until the mature phase of IOD.

These results suggest that the change of the upwelling along the south Java coast is probably the most important sources of the surface IOD variability.

According to a regional analysis of the surface heat flux anomaly, the relationship between the SST anomaly and the surface heat flux anomaly is reversed mainly because the anomalous decreasing of the SST due to the oceanic process affects the evaporation (latent heat flux) anomaly in the coastal area more strongly than the strengthen of the wind speed. Consequently, contribution of the surface heat flux to the change of the ocean temperature, and therefore the effect of the thermal coupling, is weak everywhere in the eastern pole region throughout the development of IOD. Apparently close relationship between the SST and the surface heat flux in the eastern pole region in previous works might be attributed to the overall spatial averaging of individual parameters in the eastern pole region.

The atmospheric response to the oceanic processes proposed in this study is addressed in the next study. Recently, Yuan and Liu (2009) reported that the equatorial wave propagation is related to the termination of IOD. The contribution of the remote effect through the oceanic planetary wave is another important problem.

Acknowledgments. WOCE IX1 XBT temperature data set, maintained by Bureau of Meteorology, Australia was obtained from Joint Australian Facility for Ocean Observing Systems (JAFOOS). The data used in this study have been obtained from the Data Server of "Kyousei" category #7 (k7) of "RR2002: Project for Sustainable Coexistence of Human, Nature, and the Earth" sponsored by MEXT. This study is supported by the Ministry of Education, Culture, Sports, Science and Technology, Grants-in-Aid for Scientific Research (C), 19540459, 2007.

REFERENCES

Annamalai, H., R. Murtugudde, J. Potemra, S.P. Xie, P. Liu and B. Wang, 2003: Coupled dynamics

over the Indian Ocean: spring initiation of the Zonal Mode, *Deep-Sea Res. II*, 50, 2305-2330.

Feng, M., and Meyers, G., 2003: Interannual variability in the tropical Indian Ocean: a two-year time-scale of Indian Ocean Dipole. *Deep Sea Research Part II*, 50, 2263-2284.

Harrison, D.E., and N.K. Larkin, 1998: El Niño-Southern Oscillation Sea Surface Temperature and Wind Anomalies, 1946-1993, *Rev. Geophys.*, 36,3, 353-399.

Hastenrath, S., A. Nicklis, and L. Greischar, 1993: Atmospheric-Hydrospheric Mechanism of Climate Anomalies in the Western Equatorial Indian Ocean, *J. Geophys. Res.*, 98, 20,219--20,235.

Hendon, H.H., 2003: Indonesian Rainfall Variability: Impacts of ENSO and Local Air-Sea Interaction, *J. Climate*, 16, 1775--1790

Kajikawa, Y., T. Yasunari, and R. Kawamura, 2003: The Role of the Local Hadley Circulation over the Western Pacific on the Zonally Asymmetric Anomalies over the Indian Ocean, *J. Meteor. Soc. Japan*, 81, 259-276.

Kalnay, E., M. Kanamitsu, R. Kistler, W. Collins, D. Deaven, L. Gandin, M. Iredell, S. Saha, G. White, J. Woolen, Y. Zhu, M. Chelliah, W. Ebisuzaki, W. Higgins, J. Janowiak, K.C. Mo, C. Ropelewski, J. Wang, A. Leetmaa, R. Reynolds, R. Jenne, and D. Joseph, 1996: The NCEP / NCAR 40-Year Reanalysis Project, *Bull. Amer. Meteor. Soc.*, 77, 437-471

Lau, N.-C., and M.J. Nath, 2004: Coupled GCM Simulation of Atmosphere--Ocean Variability Associated with Zonally Asymmetric SST Changes in the Tropical Indian Ocean, *J. Climate*, 17, No.2, 245--265.

Li, T., Y. Zhang, E. Lu, and D. Wang, 2002: Relative role of dynamic and thermodynamic processes in the development of the Indian Ocean dipole: An OGCM diagnosis, *Geophys. Res. Lett.*, 29, 2110, doi:10.1029/2002GL015789

McClellan, J. L., D. P. Ivanova, and J. Sprintall, 2005: Remote origins of interannual variability in the Indonesian Throughflow region from data and a global Parallel Ocean Program simulation, *J.*

- Geophys. Res.*, 110, C10013, doi:10.1029/2004JC002477.
- Meyers, G., 1996: Variation of the Indonesian throughflow and the El Niño–Southern Oscillation. *J. Geophys. Res.*, 101, 12 255–12 263.
- Mochizuki, T., N. Sugiura, T. Awaji, and T. Toyoda, 2009: Toward a better modeling of seasonal climate variations over the Indian ocean by employing a 4D-VAR coupled data assimilation approach, *Mon. Wea. Rev.* (submitted)
- Nagura, M., and M. Konda, 2007: The Seasonal Development of an SST Anomaly in the Indian Ocean and Its Relationship to ENSO. *J. Climate*, 20, 38–52.
- Reynolds, R. W., T. M. Smith, C. Liu, D. B. Chelton, K. S. Casey, and M. G. Schlax, 2007: Daily high-resolution blended analyses for sea surface temperature. *J. Climate*, 20, 5473–5496.
- Sakova, I. V., Meyers, G., and Coleman, R., 2006: Interannual variability in the Indian Ocean using altimeter and IX1-expendable bathy thermograph (XBT) data: Does the 18-month signal exist?, *Geophys. Res. Lett.*, 33, L20603, doi:10.1029/2006GL027117.
- Saji, N.H., B.N. Goswami, P.N. Vinayachandran, and T. Yamagata, 1999: A dipole mode in the tropical Indian Ocean, *Nature*, 401, No.6751, 360–363.
- Shinoda, T., M. A. Alexander, and H. H. Hendon, 2004: Remote response of the Indian Ocean to interannual SST variations in the tropical Pacific. *J. Climate*, 17, 362–372.
- Sugiura N, T. Awaji, S. Masuda, T. Mochizuki, T. Toyoda, T. Miyama, H. Igarashi and Y. Ishikawa, 2008: Development of a four-dimensional variational coupled data assimilation system for enhanced analysis and prediction of seasonal to interannual climate variations. *J. Geophys. Res.*, 113, C10017, DOI: 10.1029/2008JC004741.
- Vinayachandran, P.N., Iizuka, S., Yamagata, T., 2002: Indian Ocean dipole mode events in an Ocean General Circulation Model. *Deep Sea Res. II*, 49, 1573–1596.
- Webster, P.J., A.W. Moore, J.P. Loschnigg and R.R. Leben, 1999: Coupled ocean-atmosphere dynamics in the Indian ocean during 1997-98, *Nature*, 401, 356–360.
- Yuan, D. and H. Liu, 2009: Long wave dynamics of sea level variations during Indian Ocean Dipole events. *J. Phys. Oceanogr.*, 39, doi: 10.1175/2008JPO3900.1.